RENU2 Rocket Observations of Fine-Scale Thermal Ion Upflow, Downflow, and Temperature

N. H. Godbole[1], K. A. Lynch[2], M. Burleigh[3,4], M. R. Lessard[1], L. B. N. Clausen[5], J. Clemmons[1,6], P. A. Fernandes[7], B. A. Fritz[1,8], M. Harrington[2], D. Hysell[9], D. R. Kenward[1], J. I. Moen[5,11], K. Oksavik[10,11], T. M. Roberts[12], F. Sigernes[11], M. Zettergren[3]

[1]Space Sciences Center, University of New Hampshire
[2]Department of Physics and Astronomy, Dartmouth College
[3]Physical Sciences Department, Embry-Riddle Aeronautical University
[4]Climate and Space Sciences and Engineering Department, University of Michigan
[5]Department of Physics, University of Oslo, Oslo, Norway
[6]Aerospace Corporation
[7]ISR-1 Space Science and Applications, Los Alamos National Laboratory
[8]National Research Council Postdoctoral Research Associate resident at the U.S. Naval Research Laboratory, Washington, D.C., USA
[9]Department of Earth and Atmospheric Sciences, Cornell University
[10]Birkeland Centre for Space Science, Department of Physics and Technology, University of Bergen, Bergen, Norway
[11]Department of Arctic Geophysics, The University Centre in Svalbard, Longyearbyen, Norway
[12]NASA/JPL, Pasadena, CA

Key points

- Temporally intermittent drivers are required to model the observed thermal ion temperatures consistently with Joule heating.
- Spatially intermittent signatures are observed of ion upflow amidst overall downflow; heating and flow regions are striated and adjacent.
- A Maxwellian forward modeling procedure for the ion data interpretation is improved and a sensitivity analysis is presented.

Abstract

We present an analysis of in-situ thermal ion measurements from a cusp auroral sounding rocket. Using a forward modeling procedure, we find most-probable thermal ion temperature and parallel (field-aligned) bulk flow velocity along the trajectory. Spatially and temporally intermittent fine-scale structure in upflowing/downflowing features in the dayside cusp ionosphere are presented. We show that the observed ion temperatures are consistent with Joule heating expectations if spatially and temporally intermittent drivers and responses in the dynamic cusp environment are considered. Additionally, a forward modeling procedure for the ion data interpretation is improved and a sensitivity analysis is presented.

Keywords (auroral ionosphere, cusp ion upflow, dayside cusp thermal plasma, spatial and temporal intermittency)

1 Introduction

At the low altitudes of ionospheric sounding rockets ($\approx$ 200 km to 450 km), the predominant field-aligned motion of the ambient thermal ion population in auroral regions can be downgoing, and may indicate signatures of flux tubes with upflow at higher altitudes, or with upflow at previous times (e.g. Burleigh et al., 2019). This has been seen both as a downflowing vertex of energetic ion conics (Arnoldy et al., 1996), and as an overall downflow of the bulk thermal ion population as discussed here for the dayside case, on the nightside by Fernandes et al. (2016), and commonly throughout the polar cap by DE-2 (Loranc et al., 1991).

The Rocket Experiment for Neutral Upwelling (RENU2) was launched on December 13, 2015 at 07:34UT from the Andøya Space Center (Norway) into a neutral upwelling event to study particle behavior between 200 km and 450 km (Lessard et al., 2019). Using a forward modeling procedure (Fernandes et al., 2016; Fernandes & Lynch, 2016) and calculating Maxwellian distributions constrained by other diagnostics (e.g. GPS velocity, in situ DC electric field, radar electron density profiles, and in situ ambient electron temperature (T_e) for the spacecraft's sheath potential, denoted ϕ_{sheath}), we find the Maxwellian parameters that best compare to distribution function 2-D slices observed by a thermal ion electrostatic analyser, establishing a database of most-probable thermal ion temperature (T_i) and parallel (field-aligned) bulk flow velocity ($v_{i_\parallel}$) along RENU2's trajectory. In the Discussion section, we interpret these observations in the context of the Geospace Environment Model of Ion-Neutral Interactions with Transverse Ion Acceleration (GEMINI-TIA) 2-D ionospheric model (Burleigh & Zettergren, 2017), showing that intermittency in both drivers and responses is necessary for interpreting this event.

2 Instrumentation

We present data from the HEmispherical Energy Particle Spectrometer (HEEPS-T) (Fernandes et al., 2016), an electrostatic analyser which measures the ionospheric thermal core (energies 0.12 - 22 eV in the spacecraft frame). We use the HEEPS-T 2-D slices of the ion distribution functions to calculate temperature and parallel bulk flow velocity. While HEEPS-T data are collected at 8 Hz per energy-pitch angle frame, the thermal ion population is heavily non-gyrotropic in the payload frame. We concentrate here on the four or five slices (at an 8 Hz cadence) each payload spin period (1.8 s) where the optimal side of the HEEPS-T aperture is ram-looking. Our calculation accounts only for O^+ (16 amu).

The on-board GPS provides RENU2's position and velocity. The electric field instrument was mounted on a nearby ($\approx$ 150 m from the main payload) sub-payload dur-

ing RENU2's flight. Using 12 m tip-to-tip wire booms, and sampling at 1kHz, the electric field instrument provides high-fidelity in-situ measurements of the DC and wave electric fields (Klatt et al., 2005). These measurements are used to derive the F-region plasma $\mathbf{E}\times\mathbf{B}$ drift velocities, presented here in the Earth-Centered-Earth-Fixed (ECEF) frame, using the attitude solution and the payload's (GPS) ram velocity to translate and rotate observations from the instrument frame into the ECEF frame. The Ionization Gauge (IG) instrument (Clemmons et al., 2008) consists of a set of pressure gauges that measure thermospheric gas pressure characterizing in-situ neutral winds. As with the plasma bulk flow, these neutral winds are presented here in the ECEF frame with payload motion removed.

The Electron Retarding Potential Analyzer (ERPA) provides an estimate of ϕ_{sheath} by measuring the ambient thermal electron temperature. ϕ_{sheath} is interpreted here as $5k_bT_e$, where k_b is the Boltzmann constant, consistent with current balance expectations when sunlight and work function effects cancel each other out. (Frederick-Frost et al., 2007; Siddiqui et al., 2011). The Electron PLASma instrument (EPLAS) provides measurements of electron precipitation (Kenward et al., 2020).

Electron data from the European Incoherent SCATter (EISCAT) Svalbard 42 m radar (ESR) indicated multiple transients in temperature prior to launch, consistent with poleward moving auroral form (PMAF) activity. RENU2 was launched into the fourth of these PMAFs. Weak ion upflow can be observed in the ESR field-aligned profiles (data available at `spdf.gsfc.nasa.gov`) above 400 km throughout the interval. Between 07:34 and 07:48 UT, upflow is observed in the ESR signatures down to 300 km altitude; near 07:50 UT, downflow is seen reaching down to 250 km altitude. RENU2 entered a region of auroral precipitation at approximately T+450 s, near the 448 km apogee.

RENU2's ground track and the ESR field-aligned look direction are not common volume (though both show the same cusp event). Hence, to support the thermal ion analysis below, an altitude and geomagnetic activity dependent proxy for plasma density is generated from radar data as a function of altitude and of auroral precipitation activity level (minimal, low, and high as seen by EPLAS). When the EISCAT Very High Frequency (VHF) radar (based in Tromsø) is colocated with RENU2's trajectory (eg whenever the payload is within 200 km (or, $\approx 2^\circ$ latitude; the typical width of the cusp aurora, as on the upleg), these EISCAT VHF (Tromsø) data are used instead of ESR. Note that RENU2's closest approach to the EISCAT VHF (Tromsø) field of view occurred at T+378 s. The on-board ion observations provide a fine-scale view of the ion profiles near the event seen at larger scales by ESR (16° E longitude), and somewhat to the east (RENU2's flight trajectory spanned 16° E to 32° E longitude) within the same cusp event (trajectory detailed in Lessard et al. (2019)).

3 Maxwellian Distribution Calculations and Sensitivity Analysis

HEEPS-T measures 2-D slices of 3-D plasma distributions. Parameter-matching, using a forward-modeling procedure Fernandes et al. (2016), is utilized to characterize in-situ ion temperatures and velocities that produce the distribution. Here, we have made the assumption that the distribution is Maxwellian, which is valid at rocket altitudes ($\approx$ 200 km to 450 km), in the collisional ionosphere, for the thermal core of a distribution (Fernandes et al., 2016)). For this analysis, we assume an isotropic distribution (eg. anisotropy = 1). A previous modeling study of the RENU2 campaign predicts an anisotropy range from 0.9 to 1.1 (Burleigh et al., 2019).

First, as outlined in Fernandes et al. (2016), known parameters are constrained at each time step, including the plasma motion relative to RENU2 (calculated from DC electric field (DCE) data, GPS data, and the attitude solution), ϕ_{sheath} (from ERPA), and plasma density (from the radar data proxy). Then, an empirically determined range of

possible values for the ion temperature and parallel bulk flow velocity are allowed. Next, 3-D Maxwellian distributions are generated using the known parameters together with permutations of the possible ion temperature and parallel bulk flow velocity. These 3-D Maxwellians are translated and rotated into the payload frame, and then sliced in the 2-D plane consistent with the known attitude of the payload-mounted detector aperture at each given time step. This slice is limited to the energy range of interest (above payload potential and saturation limits, and below the top energy step of HEEPS-T).

For each possible Maxwellian at each time step, the difference (of $\log_{10}(J_E)$, where J_E is the differential energy flux; see Figure 2), between the forward-modeled Maxwellian and the data at each energy-pitch angle bin is calculated. The net summed squared difference for each possible Maxwellian slice is accumulated as a metric, and the optimal ion temperature and bulk flow velocity are selected by minimizing this metric for each time step. We note that this mean-squared difference metric provides an improved parameter search with less-scattered results than does the moment-based metric used in Fernandes et al. (2016).

Figure 1 (a) - (d) shows examples of this comparison between calculated Maxwellians and observations, for a time equatorward of the auroral precipitation (T+400.6 s, panels a and c) and for another time within the precipitation region (T+458.7 s, panels b and d). These energy-pitch angle slices are shown in the sensor frame. The output of this parameter matching at each time step (with the GPS-measured payload velocity component along the field line removed) provides the temporal profiles of $v_{i_\parallel}$ and T_i discussed in the next Section.

The sensitivity of this forward-modelling calculation to its input plasma density is illustrated by Figure 1 (e), (f). Plasma density is the most poorly-specified input parameter, hence, we focus on sensitivity to that parameter. The ESR data along the rocket trajectory upleg (not shown here) generally have higher densities than EISCAT VHF (Tromsø) data, since ESR was under the cusp aurora soft precipitation activity, and the EISCAT VHF (Tromsø) field of view was located in the subauroral zone, generally looking at the low densities of the plasma trough. Using data proxies from ESR for the total flight profile (compared with the more closely colocated EISCAT VHF (Tromsø) data for times before T+540 s) leads to an overestimate in the input plasma density by as much as a factor of 2. If used as a forward-modeling input parameter, this high density results in a reduction in the extracted ion temperature by 25% to 30% compared with the EISCAT VHF (Tromsø) driven data run, as seen in the T+300 s to T+450 s region of Figure 1 (f). The red and blue curves illustrate the effect on the extracted T_i of deliberately changing the best estimate of the density by 20%. An increase(/decrease) in the electron density input into the forward model results in a decrease(/increase) in the extracted ion temperatures.

4 Observations

Figure 2 shows the payload altitude and plasma environment (a) - (c), the forward-model-extracted thermal ion parallel-to-**B** $v_{i_\parallel}$ (with the payload GPS velocity removed) (d), and the forward-model-extracted T_i (e), all vs. flight time. The optimally matched $v_{i_\parallel}$ and T_i parameters shown here (and in Figure 1 (f) and in Figure 3 (b), (c)) have been smoothed using a seven-point moving average, roughly a 2-spin-period (3.6 s) window. Given a roughly 2 km/s payload velocity, this smoothing corresponds to 7 km resolution for static spatial structure. The parallel bulk flow velocity quantifies the ion parallel-to-**B** upflow (negative) and downflow (positive, along **B**) present along the local magnetic field. Note the prevalence of downflow with intermittent regions of localized upflow. Equatorward of the precipitation (times before T+425 s), the ions are mostly cold (≈ 0.06 eV) and downflowing (≈ 400 m/s).

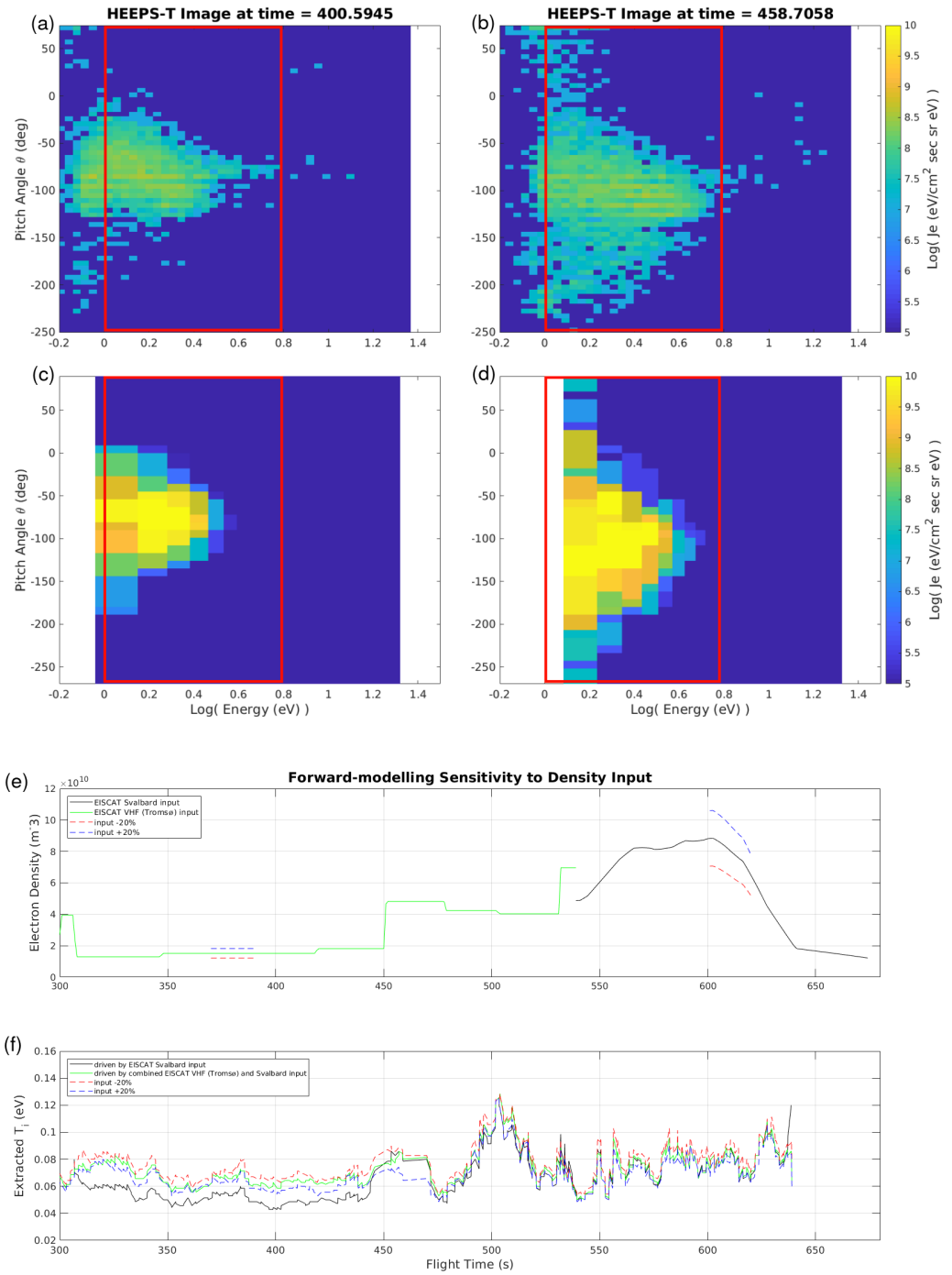

Figure 1: Maxwellian calculations: Panels (a) - (d): Parameter fitting: Measurements from HEEPS-T (a), (b) vs. the corresponding best-parameterized Maxwellian calculations (c), (d), with energy-pitch angle images presented in the sensor frame. Panels (e), (f): Forward-modelling sensitivity study: (e) different density estimates used as known inputs for the Maxwellian forward model calculation; (f) sensitivity of the algorithm to the input plasma density.

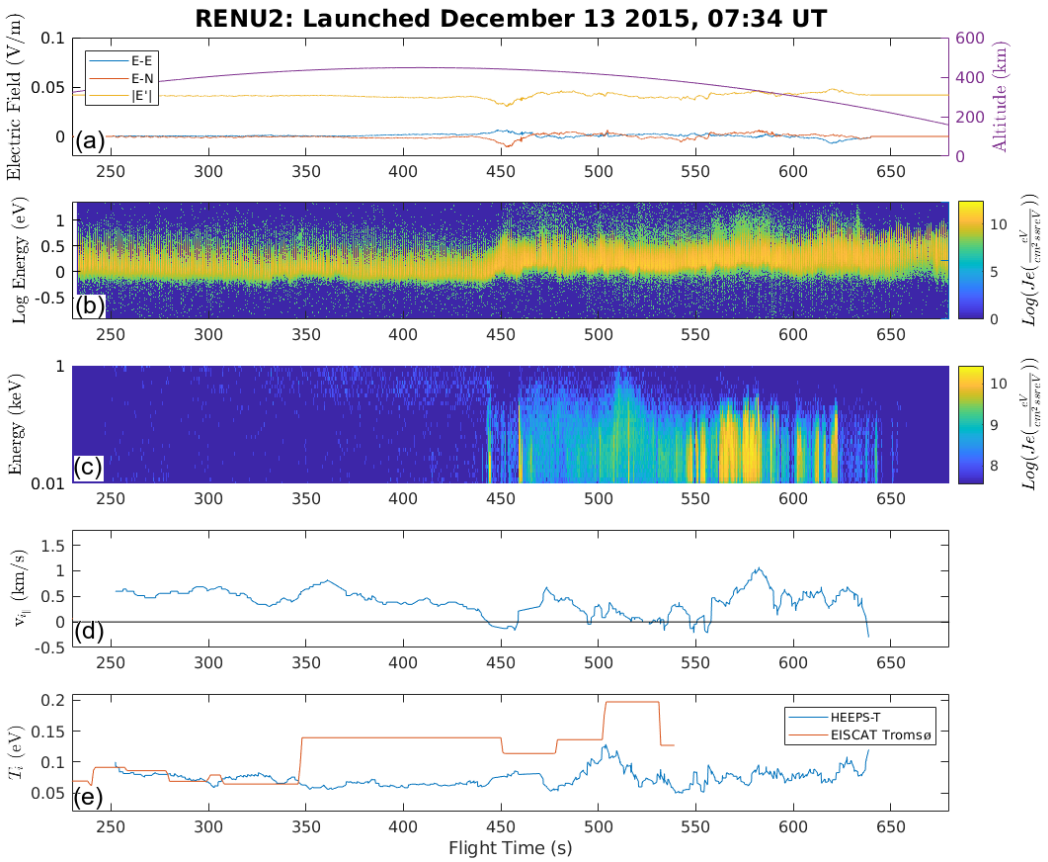

Figure 2: Stack-plot of thermal ion data in context of other diagnostics. Panel (a): in situ-observed DCE, and E' (described in text) (**E** in the ECEF frame, and E' in the neutral frame); (b) thermal ion J_E from HT for all pitch angles, in the sensor frame; (c) precipitating electron J_E from EPLAS; (d) extracted parallel-to-**B** bulk ion flow from HT, where positive values represent downflow (with the component of payload velocity along the field line removed); (e) extracted thermal ion temperature from HT, and T_i from EISCAT VHF (Tromsø).

Inside the auroral precipitation region (after T+450 s) the temperature data indicate the presence of colder temperatures interleaved with hotter, and the parallel flow velocity data indicate the presence of downflow interleaved with brief intervals of upflow. Not all hotter regions are upflowing, however. There is no local relationship between the upflow/downflow and the concurrent PMAF electron flux data (or the ELF spectral data, not shown here), as the timescales of electron precipitation and ion transport are very different.

5 Discussion

We comment on a few aspects of these observations. (1) The observed ion temperatures are only consistent with expectations for Joule heating processes if temporal and spatial variability are taken into account. (2) The prevalent parallel bulk flow velocity is downward, with brief, intermittent regions of upflow; and the regions of upflow and downflow are striated and nearby each other. (3) Rigorous modelling of such a scenario requires that temporal and spatial intermittency of both drivers and responses be considered.

First, (1), let us consider the extracted ion temperatures in the context of the environment. A common expectation for ionospheric ion temperatures is that they are related to collisional heating between the neutral and ion populations. This is typically quantified by the following relation (Schunk et al., 1975; Fernandes et al., 2016):

$$\mathbf{E}' = (\mathbf{E} + \mathbf{u_n} \times \mathbf{B}) \tag{1}$$

$$T_i = T_n + 33.0 \cdot E'^2 \tag{2}$$

Here T_i and T_n (in eV) are the ion and neutral temperatures respectively, $\mathbf{E}$ (in V/m) and $\mathbf{B}$ (in T) are the electric and magnetic fields, and $\mathbf{u_n}$ (in m/s) are the neutral velocities. We use here a magnetic field magnitude of 45,000 nT downward in the ECEF frame for the full flight duration. The neutral wind velocities are 608 m/s east, 690 m/s north throughout the flight. These values provide an upper limit for the neutral winds along RENU2's trajectory. These are much larger than the observed in-situ relative $\mathbf{E}\times\mathbf{B}$ plasma drift velocities (in the ECEF frame), which rarely exceed 100 m/s during this event. The magnitude of $\mathbf{E}'$ (equation (1)) is shown (in gold), compared with the components of $\mathbf{E}$ (orange and blue), in Figure 2(a). The observed T_n (from the IG) ranges from approximately 0.04 eV to 0.08 eV along RENU2's flight, with the average neutral temperature being approximately 0.065 eV.

Figure 3(a) shows that extracted ion temperatures are roughly bounded between $T_n + 33.0 \cdot E'^2$ and T_n. Allowing for time variable histories of $\mathbf{E}$ and $\mathbf{E}'$, this result is consistent with expectations from Joule heating processes. Note that only the average observed value for each neutral parameter is used throughout the flight and there exists no local point-to-point correlation between T_i and E'^2 as was seen previously on the nightside, where the DCE was the dominant factor (Fernandes et al., 2016). While neutral wind parameters vary slowly, plasma DCE can vary abruptly and over sharp boundaries. The in situ DCE, while of high fidelity and fine resolution, only indicate the state of the DCE at the time of the rocket passage; the radar data indicate that higher DCE values prevailed just before the rocket flight. If the earlier DCE and resulting $\mathbf{E} \times \mathbf{B}$ velocities were comparable and parallel to the neutral wind flow such that E'^2 would have been negligible (i.e., ions at rest in the neutral frame), the relative velocities in the neutral frame would be small and frictional heating would be minimized, making T_n a reasonable lower bound for T_i (given the long time history of ion heating and upflow processes). The average T_n throughout the flight was 0.065 eV as shown in the figure, but it varied between 0.04 eV and 0.08 eV. Deep within the auroral region where the plasma flow is seen to be small, the relative velocity in the neutral frame is large, and Equation 2 provides an upper bound for expected T_i. As the accompanying radars indicate a time-variable plasma flow, the range of frictional heating expected varies from very little (at times when the plasma flow may have been comparable to the neutral flow, i.e., T+350 s to T+425 s), to very large (at the time of the rocket passage, i.e., T+500 s, where the weak plasma flows are very different from the strong neutral winds), such that the observed thermal ion temperatures can be consistent with Joule heating expectations.

Next, (2), we consider the prevailing downward bulk velocity of the thermal ions, that contains localized and intermittent regions of upflow. Equatorward of the auroral electron precipitation, the thermal ions are all downflowing. It is worth noting that sufficiently strong northward neutral winds, such as the >500 m/s northward component of neutral wind observed here, can also act to suppress ion upflow, even to the point of causing downflow (Burleigh & Zettergren, 2017). In the case of the RENU2 observations, a 690 m/s northward neutral flow could account for 80-100 m/s of the bias toward downward field-aligned flow shown in Figure 2 (d), given the difference between the field line and local vertical along the trajectory ranging from 10 deg to 6 deg.

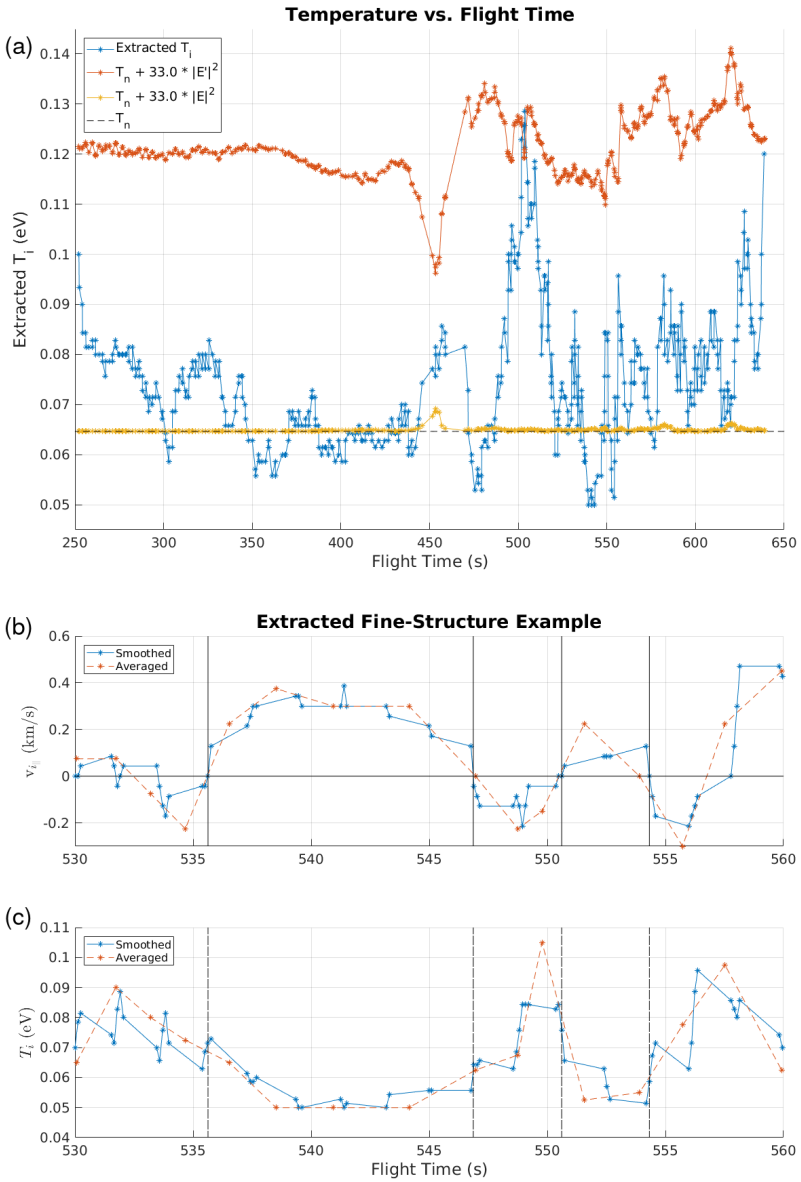

Figure 3: Panel (a): Extracted ion temperature compared with frictional heating expectations derived from in-situ DCE, and from neutral wind observations, see text. Panels (b), (c): Close-up of fine-structure in the extracted ion parameters, as discussed in Point (2). Data shown in this closeup panel include unsmoothed data points (orange) averaged over 4 samples, roughly a one-spin (1.8 s) cadence.

Within the cusp precipitation, there are localized embedded regions of upflow within this downflow. Figure 3 (b), (c) details the localized transitions from a cold, downflowing region (T+535.6 s to T+546.8 s) to a warmer, upflowing region (T+546.8 s to T+550.6 s), followed by another downflowing region (T+550.6 s to T+554.3 s). In this closeup plot we show both the seven-point-moving-average values (blue) together with four-point-average values with a one-spin (1.8 s, 4 km) resolution. Assuming Doppler-shifted spatial structuring, the first region is approximately 26 km in extent, the second region is approximately 9 km in extent, while the third region is approximately 7 km in extent. Note the

narrow confinement of the heated upflowing ion structures, and their adjacence to colder downflowing structures. These sharp transitions motivate the spatially bounded localized driver explored in the point (3) below, given the time needed to change ion population parameters.

Downflow at these altitudes can be an indication of upflow either at higher altitudes, or at earlier times. As an aside, we note that another thermal ion instrument on RENU2, which roughly separates H^+ from heavier ions, shows a clear localized proton downflow event between T+346 and T+348 s. This can be interpreted as the result of a previously heated flux tube that was previously within the cusp activity, which at the time of the rocket passage is found just equatorward of the existing precipitation boundary. If the flux tube was recently heated by activity, but at the time of the observation the driver has moved away, as is often the case with PMAFs, the H^+ would return to lower altitudes after having failed to receive the energy necessary to cause it to outflow. This proton-specific, localized event is a case for future study.

Thirdly, (3), we discuss the spatial and temporal intermittency required, for both drivers and responses, to quantify an event such as seen by RENU2. Loranc et al. (1991), in interpreting DE-2 observations of vertical flows at high latitudes, put their observations in the context of localized, convecting flux tubes of frictional heating. Here we investigate quantifying such a scenario specifically for the localized regions of upflow seen in the RENU2 observations, using the GEMINI-TIA model (Burleigh & Zettergren, 2017). The time evolution required for ion heating and upflow, coupled with the small scales of the localized regions, means that the drivers and the responses may not be co-located in time or space. However, the sharp boundaries observed make inferences about spatial structuring reasonable, and the large temperature changes observed constrain modelled parameters. Figure 4 illustrates one such scenario, where a localized flux tube (0.3 deg wide) is driven with frictional heating imposed by a localized region of DCE (40 mV/m) for a short period of time (60 sec). The driver is sufficient to raise the local ion temperature to the observed values, and the hysteresis on the flux tube allows the effects of this heating to remain for 30-60 s after the driver is turned off.

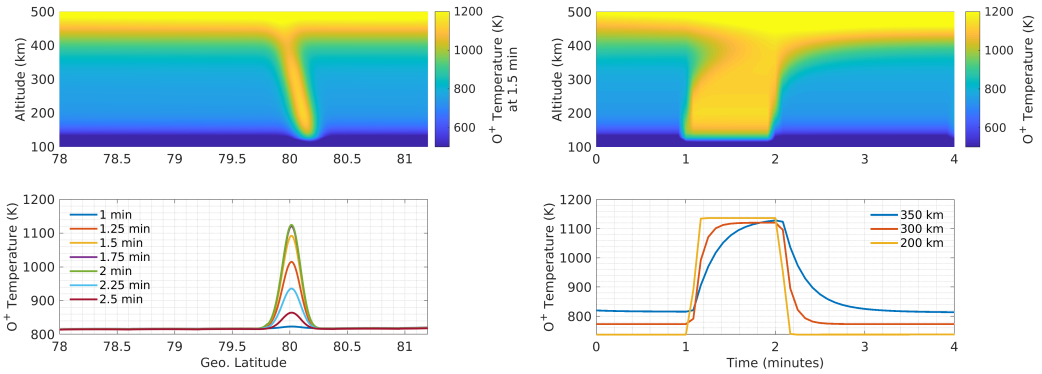

Figure 4: A GEMINI-TIA simulation of spatially and temporally intermittent frictional heating. A DCE of 40 mV/m is applied over a 0.3 deg region for 60 seconds (from T+1 min to T+2 min.) The upper left panel shows the heated flux tube at T+1.5 min, and the lower left panel shows profile cuts at 350 km altitude at a sequence of times. The heating region remains locally confined. The right panels show the time evolution along the center of the heated flux tube. The heating moves up from the E-region to fill the entire flux tube within a few 10s of sec, and remains at the upper end of the flux tube for up to a minute after the driver is removed.

6 Conclusions

While this GEMINI-TIA simulation can reproduce features seen in the observations, a full system-level quantification of such a cusp event requires a more complete data set to drive it. For this simulation we have chosen a localized frictional heating DCE driver region consistent with the lower limit of imagery scale sizes shown in Burleigh et al. (2019) and Lessard et al. (2019); the 0.3 deg extent of the simulated driver is also comparable to the FWHM scale of the DCE event shown in Fig 2(a), assuming a spatial structure. The simulated DCE has a strength (40 mV/m) sufficient to raise the ion temperature through Joule heating by 300 K, the range of temperatures shown in Figure 3(a). A full simulation of an event such as this requires multipoint in situ driving data at fine resolution over a 2-D region, on the temporal and spatial scales and durations of the various processes. Single-point in situ observations in the context of imagery can illustrate features but it remains difficult to quantify the net effect of this intermittent driving, with its intermittent responses, in terms of overall outflow, without reasonable inferences to extend the fine-scale observations in space and time. Modern three-dimensional ionospheric models such as GEMINI (Zettergren & Semeter, 2012) can model the ionospheric heating volume. However, multipoint in situ observations that can separate the spatial and temporal variations glimpsed by these observations and by those such as Oksavik et al. (2004) and Moen et al. (2004), are needed to drive the model for conclusive quantification. A complete modelling quantification of the calculated upflow response requires observations on a distributed grid, with observations covering the various spatial and temporal scales and durations of the heating process evolution illustrated in the simple simulation here. A full characterization, thus, awaits the development of truly multipoint in situ observations for both the drivers, and the responses.

Acknowledgments

Support was provided at the University of New Hampshire by NASA award NNX13AJ94G, at Dartmouth College by NASA award NNX13AJ90G, and from the Research Council of Norway grants 275653 and 223252. MB was supported by NSF CAREER grant AGS-1255181 and NASA grant 80NSSC17K0015. Data from the RENU2 sounding rocket mission are publicly available at NASA's Space Physics Data Facility (spdf.gsfc.nasa.gov). EISCAT is an international association supported by research organisations in China (CRIRP), Finland (SA), Japan (NIPR and ISEE), Norway (NFR), Sweden (VR), and the United Kingdom (UKRI). The data were obtained from https://www.eiscat.se. KAL thanks David Collins, Dwayne Adams, and Ralph Gibson for their engineering support, and WFF/NSROC personnel for their dedication to the rocket program and efforts in performance analysis. BF is supported by the Chief of Naval Research. The authors thank the Editor and previous reviewers for their constructive commentary.

References

Arnoldy, R. L., Lynch, K. A., Kintner, P. M., Bonnell, J., Moore, T. E., & Pollock, C. J. (1996). SCIFER Structure of the Cleft Ion Fountain at 1400 km altitude. *Geophysical Research Letters*, *23*(14), 1869-1872. doi: 10.1029/96GL00475

Burleigh, M., Zettergren, M. Lynch, K. A., Lessard, M. R., Moen, J., Clausen, L. B. N., ... Liemohn, M. (2019). Transient Ionospheric Upflow Driven by Poleward Moving Auroral Forms Observed During the Rocket Experiment for Neutral Upwelling 2 (RENU2) Campaign. *Geophysical Research Letters*.

Burleigh, M., & Zettergren, M. (2017). Anisotropic fluid modeling of ionospheric upflow: Effects of low-altitude anisotropy and thermospheric winds. *Journal of Geophysical Research: Space Physics*, *122*(1), 808-827. doi: 10.1002/2016JA023329

Clemmons, J. H., Hecht, J. H., Salem, D. R., & Strickland, D. J. (2008). Thermospheric density in the Earth's magnetic cusp as observed by the Streak mission.

Geophysical Research Letters, *35*(24). doi: 10.1029/2008GL035972

Fernandes, P. A., & Lynch, K. A. (2016). Electrostatic analyzer measurements of ionospheric thermal ion populations. *Journal of Geophysical Research: Space Physics*, *121*(7), 7316-7325. doi: 10.1002/2016JA022582

Fernandes, P. A., Lynch, K. A., Zettergren, M., Hampton, D. L., Bekkeng, T. A., Cohen, I. J., ... Powell, S. P. (2016). Measuring the Seeds of Ion Outflow: Auroral Sounding Rocket Observations of Low-Altitude Ion Heating and Circulation. *Journal of Geophysical Research: Space Physics*, *121*(2), 1587-1607. doi: 10.1002/2015JA021536

Frederick-Frost, K. M., Lynch, K. A., Kintner Jr., P. M., Klatt, E., Lorentzen, D., Moen, J., ... Widholm, M. (2007). SERSIO: Svalbard EISCAT Rocket Study of Ion Outflows. *Journal of Geophysical Research: Space Physics*, *112*(A8). doi: 10.1029/2006JA011942

Kenward, D. R., Lessard, M. R., Fritz, B. A., Oksavik, K., Lynch, K. A., Roberts, T. M., ... Sigernes, F. (2020). Characterization of Soft Electron Precipitation in the Cusp Region During Poleward Moving Auroral Form Event. *submitted, Geophysical Research Letters*.

Klatt, E. M., Kintner, P. M., Seyler, C. E., Liu, K., MacDonald, E. A., & Lynch, K. A. (2005). SIERRA Observations of Alfvénic Processes in the Topside Auroral Ionosphere. *Journal of Geophysical Research: Space Physics*, *110*(A10). doi: 10.1029/2004JA010883

Lessard, M. R., Fritz, B. A., Sadler, B., Cohen, I. J., Kenward, D. R., Godbole, N. H., ... Yeoman, T. (2019). Overview of the Rocket Experiment for Neutral Upwelling Sounding Rocket 2 (RENU2). *Geophysical Research Letters*. doi: 10.1029/2018GL081885

Loranc, M., Hanson, W. B., Heelis, R. A., & St.-Maurice, J.-P. (1991). A morphological study of vertical ionospheric flows in the high-latitude F region. *Journal of Geophysical Research: Space Physics*, *96*(A3), 3627-3646. doi: 10.1029/90JA02242

Moen, J., Oksavik, K., & Carlson, H. C. (2004). On the Relationship Between Ion Upflow Events and Cusp Auroral Transients. *Geophysical Research Letters*, *31*(11). doi: 10.1029/2004GL020129

Oksavik, K., Sø raas, F., Moen, J., Pfaff, R., Davies, J., & Lester, M. (2004, 01). Simultaneous optical, CUTLASS HF radar, and FAST spacecraft observations: Signatures of boundary layer processes in the cusp. *Ann. Geophys.*, *22*. doi: 10.5194/angeo-22-511-2004

Schunk, R. W., Raitt, W. J., & Banks, P. M. (1975). Effect of Electric Fields on the Daytime High-Latitude E and F Regions. *Journal of Geophysical Research*, *80*(22), 3121-3130. doi: 10.1029/JA080i022p03121

Siddiqui, M. U., Gayetsky, L. E., Mella, M. R., Lynch, K. A., & Lessard, M. R. (2011). A Laboratory Experiment to Examine the Effect of Auroral Beams on Spacecraft Charging in the Ionosphere. *Physics of Plasmas*, *18*, 092905-092905. doi: 10.1063/1.3640512

Zettergren, M., & Semeter, J. (2012). Ionospheric plasma transport and loss in auroral downward current regions. *Journal of Geophysical Research: Space Physics*, *117*(A6).